Quantification of crack area in ceramic matrix composites at single-fiber push-out testing and influence of pyrocarbon fiber coating thickness on interfacial fracture toughness

W.M. Mueller*, J. Moosburger-Will, M.G.R. Sause, M. Greisel, S. Horn

University of Augsburg, Institute of Physics, Experimental Physics II, 86135 Augsburg, Germany

Abstract

For mechanical characterization of interfacial properties in fiber-reinforced ceramic matrix composites by single-fiber push-out tests, a determination of the relevant crack area is required. In established evaluation methods, the relevant crack area is approximated by the total cylindrical fiber surface of the pushed fiber. This concept disregards that stable crack propagation, which is relevant for prediction of macromechanical behavior, may occur on just part of the fiber-matrix interface area. In the present publication, a new approach to quantify the relevant crack area is presented, enabling a more reliable determination of the interfacial fracture toughness of ceramic matrix composites.

The new concept is applied to SiC-fiber reinforced SiC-matrix composites with pyrocarbon fiber coatings (SiC/PyC/SiC) produced via chemical vapor infiltration technique. The occurrence of stable and unstable crack growth, as predicted in literature, can be verified experimentally. A strong correlation between PyC fiber coating thickness and interfacial fracture toughness is found.

Keywords: Single-fiber push-out test; Crack area; Interfacial fracture toughness; Pyrocarbon fiber coating; Composites

1. Introduction

Ceramic matrix composites (CMC) have found their way as structural materials into a wide field of applications in harsh environments, involving high temperatures, high stress levels and corrosive atmospheres. The fields of application include the areas of aerospace, ground transportation, power generation and chemical industries. It is widely accepted that the mechanical properties of fiber-reinforced ceramic matrix composites are closely related to the fiber-matrix interfacial properties [1,2]. In particular, the interfacial fracture toughness is considered to be one of the most relevant quantities to characterize the material behavior at the fiber-matrix interface of a composite sample under mechanical load [3]. In silicon carbide fiber-reinforced silicon carbide matrix composites (SiC/SiC), fiber-matrix interfacial properties are modified by fiber coatings which facilitate fiber-matrix debonding and thus micro-crack deflection at the fiber-matrix interface. Today, pyrolytic carbon (PyC) coatings applied by a chemical vapor deposition process are predominantly used in technical applications.

The single-fiber push-out test plays a major role in the micromechanical characterization of the interfacial properties since its introduction by Marshall [4,5] in 1984 [6–14]. Recently, a modification of the single-fiber push-out test was published by our group [15], enabling a quantification of the energy dissipated by stable crack propagation during debonding of fiber and matrix.

However, the corresponding crack area is usually simply estimated by the total cylindrical fiber surface area of the pushed fiber. Since the occurrence of both, stable and unstable crack propagation is expected [3], the existing approximations represent an upper limit of the actual relevant area of stable crack growth.

In the present publication, a new approach to quantify the relevant crack area is presented. It is based on a quantification

* Corresponding author. Tel.: +49 821 598 3453; fax: +49 821 598 3411.
E-mail address: wolfgang.mueller@physik.uni-augsburg.de (W.M. Mueller).

of the crack energy dissipated during crack growth as a function of the total sample thickness. The enhanced quantification of the crack area leads to a more reliable determination of the interfacial fracture toughness of the samples.

In previous push-out studies [8,10], it has been shown that the PyC coating thickness is a parameter to influence fiber-matrix interfacial properties, e.g. the interfacial shear strength. In the current publication, a correlation between the PyC fiber coating thickness and the interfacial fracture toughness of SiC/PyC/SiC composites is investigated for the first time. To this end, the new push-out evaluation method presented here is applied to SiC/PyC/SiC composites with PyC fiber coatings of three different thicknesses and the effect on the interfacial fracture toughness is discussed.

2. Experimental

2.1. Material and sample preparation

The samples investigated in the present study are SiC-fiber (Tyranno Grade S, Ube Industries, Ltd.) reinforced SiC-matrix composites with PyC fiber coatings. The samples were produced from plain-woven SiC-fiber fabrics via chemical vapor infiltration (CVI) method by a two-step procedure to deposit a PyC coating on the fibers and, subsequently, to form the SiC-matrix. In the present study, three types of CMC samples are investigated, which differ from each other in their fiber coating thickness. The coating thickness of the three samples was measured via scanning electron microscopy (SEM) on polished cross sections. The measurement was performed on 15 fibers per sample type with 2 positions per fiber. The coating thickness was taken as the distance of two parallel straight lines, which were aligned tangentially to the fiber-coating and coating-matrix interface, respectively. The thickness and standard deviation turned out to be (75 ± 5) nm, (40 ± 3) nm and (20 ± 5) nm, respectively (see Fig. 1). In the following sections, they are referred to as PyC-A, PyC-B and PyC-C. The samples were provided by MT Aerospace AG.

For the push-out tests, the samples need to be thinned to an appropriate thickness (typical below 150 μm) with plane-parallel surfaces orientated perpendicular to the fiber axis direction. This was done by a multi-stage thinning process, including a precision low speed cutting process (Isomet, Buehler), a lapping process (Precision Lapping and Polishing System PM5, Logitech Ltd.) with boron carbide particles (grain size 9 μm) and a final polishing step with a colloidal silica sol.

From each sample type (PyC-A, PyC-B, PyC-C) push-out samples of different thicknesses were prepared: Sample PyC-A was thinned to obtain four push-out samples having a thickness of 68 μm, 76 μm, 94 μm and 128 μm, respectively. From sample type PyC-B, push-out samples with a thickness of 60 μm and 85 μm were prepared. Sample PyC-C was thinned to obtain an 86 μm and an 102 μm thick push-out sample. The thickness of the samples has been measured by a height gauge and by optical microscopy. The deviations in thickness resulting from multiple measurements with both methods turned out to be less than 1 μm. An overview of the samples is given in Table 1. The samples cover a maximum range of feasible sample thicknesses for the push-out tests, being limited by the mechanical stability of the composite samples on the one hand and the fiber compressive strength on the other hand.

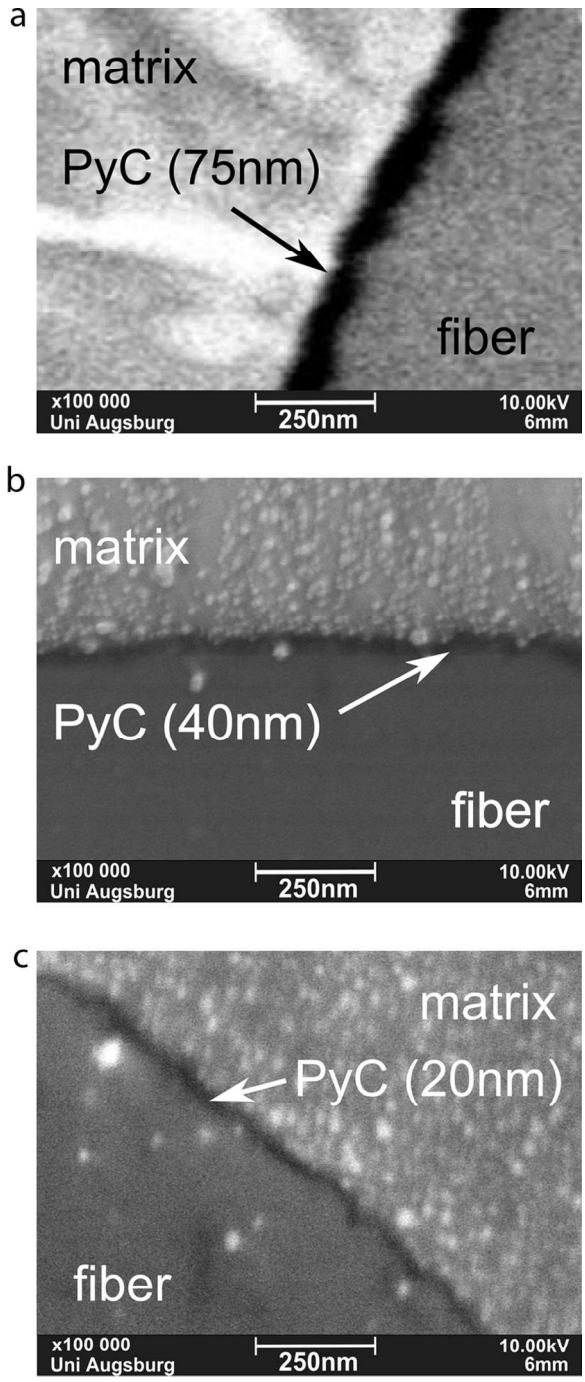

Fig. 1. SEM analysis of the PyC fiber coating on polished cross sections of the SiC/PyC/SiC samples (magnification 100,000×). (a) Sample PyC-A, (b) sample PyC-B and (c) sample PyC-C.

For carrying out the push-out tests, the specimens were then placed on a glass substrate with a groove of 60 μm in width, and fixed by quartz wax ensuring close and stiff contact to the substrate.

Table 1
Overview of SiC/PyC/SiC samples investigated by single-fiber push-out testing.

Sample	Coating thickness	Sample thickness
PyC-A	(75 ± 5) nm	68 μm 76 μm 94 μm 128 μm
PyC-B	(40 ± 3) nm	60 μm 85 μm
PyC-C	(20 ± 5) nm	86 μm 102 μm

2.2. *Single-fiber push-out test with unloading-reloading cycle*

The single-fiber push-out tests were performed using an Universal Nanomechanical Tester system (Asmec GmbH), enabling displacement-controlled experiments with a force measurement resolution of 0.01 mN and a resolution of normal displacement of 1 nm. The lateral positioning accuracy of the indenter tip was about 1 μm. In the current study, a flat-end indenter tip was used. The tip had the shape of a truncated four-sided pyramid with an edge length of 4.0 μm and a total included angle of 38.3° (Microstar Technologies). In previous studies of our group [15,16] it was shown that this tip geometry allows to perform single-fiber push-out tests without the indenter touching the matrix throughout the process.

In the current study, the single-fiber push-out tests were performed following the approach of Refs. [15,16]. This procedure requires the implementation of an unloading-reloading cycle within the loading schedule for quantification of the energy dissipated by stable crack growth during the test. The procedure is applicable in the case that there is a distinct signature in the load-displacement curve which can be associated with crack initiation and, additionally, that plastic deformation of the matrix can be neglected. This behavior is typical for ceramic matrix composites. Recently, this approach was expanded to samples with a more ductile matrix, e.g. for carbon-fiber reinforced polymers, leading to substantial plastic matrix deformation during the test and to crack initiation without a distinct signature in the load–displacement curve [17–19].

The push-out tests were performed under displacement-controlled mode. The loading schedule (Fig. 2) consists of one unloading-reloading cycle and a maximum indenter displacement of 3.0 μm. The position of the start of the unloading cycle was adapted to the failure behavior of the samples and was varied between an indenter displacement of 1.0 and 1.8 μm. The loading segments were performed at a displacement rate of 50 nm/s, whereas the unloading segments were performed at a rate of 100 nm/s. At maximum indenter displacement, a dwell time of 10 s was set.

The tested fibers were selected randomly in a sample area of several mm^2, comprising fibers with different configurations with respect to the number of nearest neighboring fibers (Fig. 4 and 5).

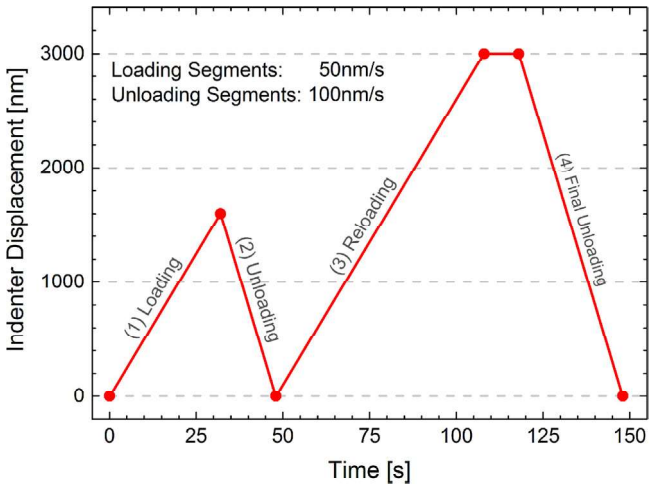

Fig. 2. Typical loading schedule for push-out testing of the SiC/PyC/SiC samples, including an unloading-reloading cycle at an indenter displacement of 1.6 μm for the evaluation of the dissipated energy [15,16].

3. Results and discussion

3.1. *Load–displacement curve*

In Fig. 3, a typical load–displacement curve of a single-fiber push-out test is shown. It was performed on a sample of type PyC-B with a thickness of 85 μm. The load–displacement graph exhibits the characteristics that have been previously described for displacement-controlled measurements performed with flat-end indenter tips [15]. The initial rise of the curve (up to 175 mN) is attributed to elastic deformation of fiber and matrix, and plastic deformation of the fiber top surface. At an indenter displacement of 430 nm (load: 175 mN), there is a distinct change in slope of the curve which is attributed to crack initiation at the fiber-matrix interface. This is followed by an extended linear segment of the load signal which is dominated by stable crack propagation [15]. At an indenter displacement of 1.6 μm, an unloading-reloading cycle is inserted to evaluate the different energy contributions. At maximum load of 415 mN, stable crack propagation turns to

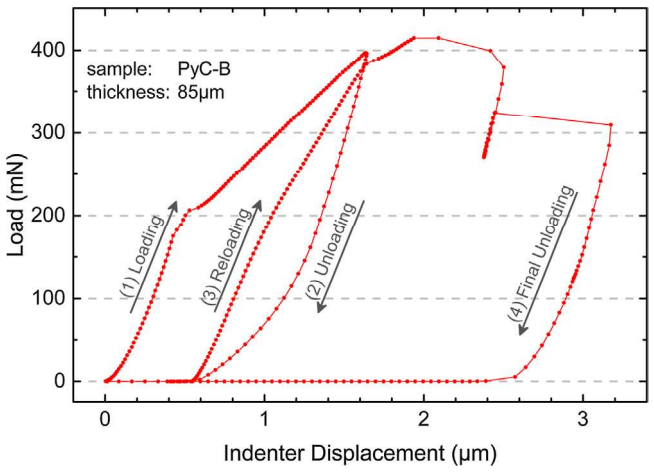

Fig. 3. Load–displacement curve of a single-fiber push-out test performed on a sample of type PyC-B (sample thickness 85 μm).

unstable propagation, which almost instantly results in complete fiber-matrix debonding and a fiber displacement relative to the sample surface on front and back side ('fiber push-out'). The abrupt fiber displacement is accompanied by a decrease in load and results in a narrow loop caused by the displacement control unit (indenter displacement: 2.5 μm). The final unloading segment of the curve was set before the indenter could affect the matrix, at a maximum indenter displacement of 3.0 μm.

3.2. Scanning electron microscopy analysis

A SEM analysis on polished cross sections of the front and back side of the samples has been conducted. In Fig. 4, the results of the front side analysis are shown.

Performing a comparison between different fibers of the same sample by SEM confirms that the thickness of the PyC fiber coatings applied via the CVD technique is homogeneous (Fig. 4(a)). Moreover, the coating thickness of a single fiber along its circumference also appears highly homogeneous based on micrographs taken at moderate magnifications that represent the entire fiber cross section (Fig. 4(a)). For high magnifications (i.e. on a scale on which the fiber surface roughness appears), however, a substantial variation in coating thickness (Fig. 1(a)) is visible, which can be attributed to the effects of fiber surface topography. Since for the evaluation of the interfacial fracture toughness the behavior of stress field and crack propagation are not considered down to the scale of the fiber roughness, the effect of the coating thickness variation is assumed to be of minor influence for the results presented.

After carrying out the single-fiber push-out tests, the tested fibers appear in dark color on the SEM images of the sample front side which indicates that they are displaced relative to the sample surface (Fig. 4(a)). Apart from an almost rectangular imprint of the flat-end indenter tip, no further damage on the fiber surface is found. In a previous publication of our group concerning the energy contributions at push-out testing [15], the energy attributed to the formation of the fiber imprints was investigated by a combination of indentation testing, scanning electron and atomic force microscopy on the same grade of SiC-fibers as used here (Tyranno Grade S). The investigation has revealed that the energy contribution for plastic deformation of the fiber top surface is negligible compared to the other energy contributions involved. There is no evidence of any contact between the indenter tip and the surrounding matrix or of plastic matrix deformation from the micrographs.

SEM micrographs of the back side of the samples taken after the tests at an angle of 45° to the sample surface, are shown in Fig. 5.

The pushed fibers are clearly protruding from the sample surfaces. The debonded fiber-matrix interfaces appear to be smooth according to the SEM images. The micrographs are in total agreement with the microscopic analysis presented in [15,16].

3.3. Crack areas of stable and unstable crack propagation

During single-fiber push-out testing, the loaded fiber is debonded by the propagation of a crack. The propagation of a crack may proceed either by stable or unstable crack propagation. Stable crack growth requires externally supplied energy for a gradual progression of the crack. In contrast, unstable crack propagation is associated with a release of energy and usually proceeds much faster, potentially reaching acoustic

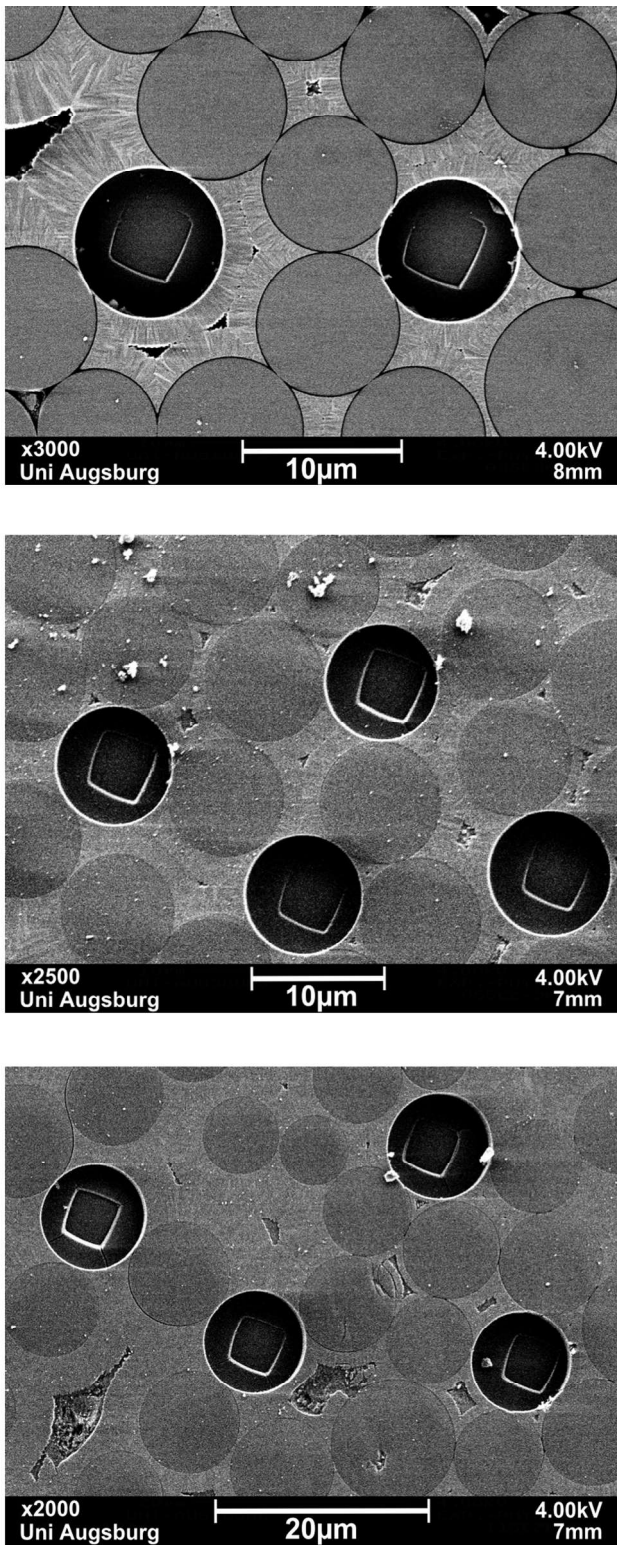

Fig. 4. SEM analysis of the front sides of the SiC/PyC/SiC samples after single-fiber push-out testing (different magnifications). (a) Sample PyC-A, (b) sample PyC-B and (c) sample PyC-C.

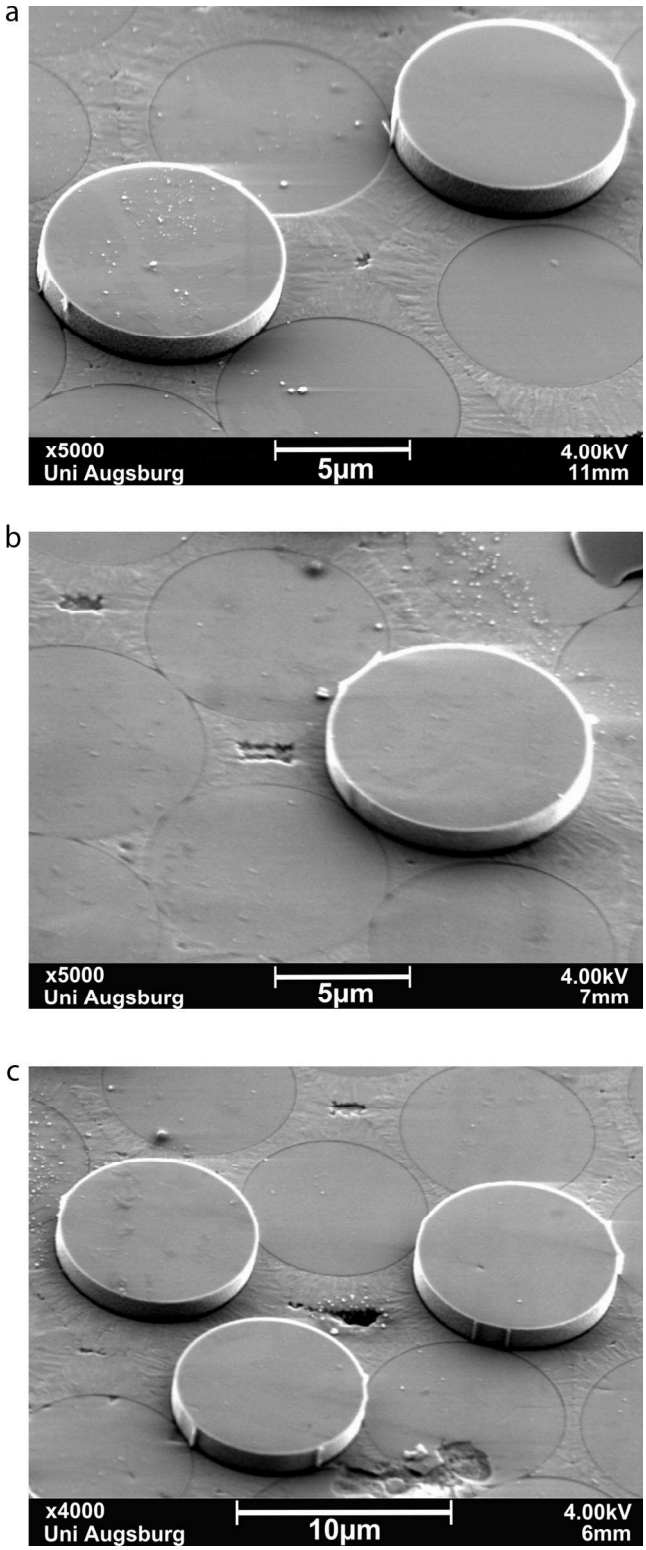

Fig. 5. SEM analysis of the back sides of the SiC/PyC/SiC samples after single-fiber push-out testing (different magnifications). (a) Sample PyC-A, (b) sample PyC-B and (c) sample PyC-C.

propagation velocities [20,21]. According to stress-based models of the single-fiber push-out test, e.g. the approach of Kerans and Parthasarathy [3], a sequence of stable und unstable crack growth is expected during debonding of the fiber.

At the beginning of the experiment, a crack between fiber and matrix is initiated at the front side of the sample by loading the fiber with an increasing force [15]. After crack initiation, the crack propagates along the interface due to the further increasing load. As the main intensity of the stress field is located close to the crack tip, the crack propagation is not affected by an interaction of the stress field with the sample back surface at an early stage of the experiment and the debonding process is dominated by stable crack propagation [22].

As the crack tip approaches the back surface of the sample, the stress field is increasingly affected by the geometric constraints, i.e. the sample back surface, which eventually leads to a transition from stable to unstable crack propagation [22]. During the unstable crack growth, the energy which has been stored elastically in the sample during loading, is released. The length of the unstable crack growth L_{unst} depends on the actual stress distribution and, therefore, is not easy to predict accurately. According to the considerations of Kerans and Parthasarathy [3], the unstable crack length is expected to be independent of the sample thickness and to be in the range of several fiber diameters.

As the stable debonding process is dominated by interfacial properties and is much less affected by geometric effects than the unstable one, the characterization of the stable process is most relevant for the prediction of macroscopic failure behavior. The debonding behavior is characterized using the interfacial fracture toughness $\langle G \rangle$, which is related to the strain energy release rate G. The strain energy release rate G is defined as the strain energy ∂U dissipated during infinitesimal crack growth per unit of newly created fracture surface area ∂A [22]

$$G = -\frac{\partial U}{\partial A} \tag{1}$$

The interfacial fracture toughness $\langle G \rangle$ is taken as the energy release rate G averaged over the area of stable crack growth $A_{\mathrm{crack,st}}$, in accordance with Refs. [15,17]. Then, the averaged energy release rate $\langle G \rangle$ is equal to the ratio of the total energy $\Delta E_{\mathrm{crack,st}}$ dissipated during the stable crack growth and the corresponding crack surface $A_{\mathrm{crack,st}}$ created in this process:

$$\langle G \rangle = -\langle \frac{\partial U}{\partial A} \rangle_{A_{\mathrm{crack,st}}} = -\frac{\Delta E_{\mathrm{crack,st}}}{A_{\mathrm{crack,st}}} \tag{2}$$

The energy contribution $\Delta E_{\mathrm{crack,st}}$ can be determined by the modified push-out procedure presented in Refs. [15,16]. The corresponding crack area $A_{\mathrm{crack,st}}$, however, so far is taken as the total cylindrical fiber surface area A_{total} of the pushed fiber (with radius r_{f} and sample thickness L) in established evaluation concepts:

$$A_{\mathrm{crack,st}} = A_{\mathrm{total}} = 2\pi r_{\mathrm{f}} L \tag{3}$$

Since the total cylindrical crack area A_{total} consists of the sum of the area of stable crack growth $A_{\mathrm{crack,st}}$ and the area of unstable crack growth $A_{\mathrm{crack,unst}}$, this approximation actually represents an upper limit of the relevant crack area. Thus, for a more precise determination of the crack area, Eq. (3) modifies to

$$A_{\mathrm{crack,st}} = A_{\mathrm{total}} - A_{\mathrm{crack,unst}} = 2\pi r_{\mathrm{f}}(L - L_{\mathrm{unst}}) \tag{4}$$

Here L_{unst} denotes the length of unstable crack growth.

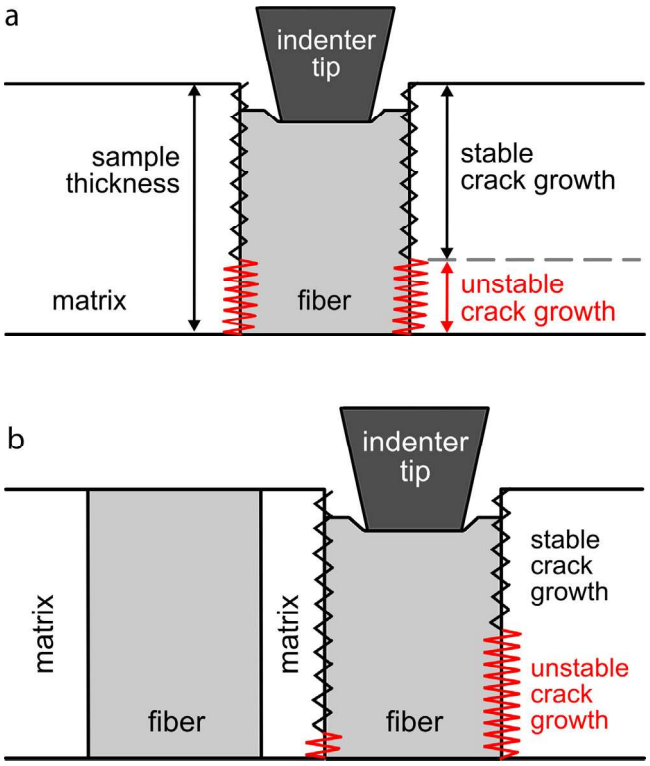

Fig. 6. Schematic illustration of the areas of stable and unstable crack growth during single-fiber push-out test in a symmetric and an asymmetric fiber configuration. (a) Symmetric fiber configuration and (b) asymmetric fiber configuration.

This approach was originally published for ceramic matrix composites in Ref. [16]. Recently, Greisel et al. [17] successfully applied this approach to carbon fiber-reinforced thermoplastic composites.

Fig. 6(a) shows a schematic illustration of the areas of stable and unstable crack growth on the fiber-matrix interface in case of one isolated fiber surrounded homogeneously by matrix material. As the stress field is symmetric with respect to the fiber axis in this configuration, the crack propagates symmetrically, leading to cylindrical shaped areas of stable and unstable crack growth. In Fig. 6(a), stable and unstable crack propagation is represented by small and large zigzag lines, respectively. In case of a symmetrical configuration, the definition of the length of stable and unstable crack propagation (L_{st} and L_{unst}) is, therefore, straightforward.

Fig. 6(b) illustrates the more general case with a neighboring fiber breaking the cylindrical symmetry of the arrangement with respect to the loaded fiber. This configuration results in a higher stress concentration in the narrow region between the fibers and, consequently, leads to stable crack growth along the interface in that region at an early stage of the experiment [19]. With increased loading, the crack propagates in fiber axis direction until it reaches the back surface of the sample. At this point of the experiment, the crack has not yet fully developed in circumferential direction [19]. With further increase of load, the remaining unaffected part of the fiber-matrix interface is debonded by stable and unstable crack growth (Fig. 6(b)). In the case of non-symmetric crack propagation, the length of stable and unstable crack propagation L_{st} and L_{unst} are no longer identified with the actual contour of the crack areas, but still are a measure of $A_{crack,st}$ and $A_{crack,unst}$. In that case, L_{st} and L_{unst} can be regarded as virtual crack lengths satisfying the conditions

$$L_{st} = \frac{A_{crack,st}}{2\pi r_f} \tag{5}$$

and

$$L_{unst} = \frac{A_{crack,unst}}{2\pi r_f} \tag{6}$$

respectively. For the following approach, there is no difference whether the crack length is regarded as a physical or a virtual quantity. It should be mentioned that the crack areas are approximated by idealized surfaces here, neglecting any surface area contributions due to the roughness of the interfaces [23,24]. Since the crack surfaces have been found to be quite smooth (see Fig. 5), this approximation seems to be appropriate.

From an energy-based point of view, the crack growth turns from stable to unstable propagation at that moment when the energy stored elastically in the fiber exceeds the energy required to overcome the remaining fiber-matrix bonding. The required energy is a function of the total amount of the remaining fiber-matrix interfacial area (i.e. the area of unstable crack growth $A_{crack,unst}$), but independent of its shape.

The local fiber configuration has an influence on the local stiffness of the sample which is effective during push-out testing. As a result, at same indenter displacement more elastic energy is stored in the sample when performing a push-out test in a sample area with higher local fiber volume content compared to an area with lower local fiber volume content. Although this behavior is reflected by a larger slope in the load–displacement curve, it does not change the dissipative energy contribution required for fiber-matrix debonding.

In summary, the local fiber configuration does influence the local stress distribution, the shapes of stable and unstable crack areas at the fiber-matrix interface, and the load–displacement curve, but does not influence the total amount of the crack areas $A_{crack,st}$ and $A_{crack,unst}$, and the energy required for fiber-matrix debonding $\Delta E_{crack,st}$.

With Eqs. (4) and (2), the interfacial fracture toughness is equal to

$$\langle G \rangle = -\frac{\Delta E_{crack,st}}{2\pi r_f (L - L_{unst})} \tag{7}$$

This equation includes two unknown parameters, $\langle G \rangle$ and L_{unst}. Assuming L_{unst} is independent of sample thickness, Eq. (7) can be regarded as a linear equation for $\Delta E_{crack,st}$ as a function of L:

$$-\frac{\Delta E_{crack,st}}{2\pi r_f} = \langle G \rangle \cdot (L - L_{unst}) \tag{8}$$

This linear relationship is illustrated in Fig. 7. In this diagram, the straight line describes the expected relation between the total energy dissipated by stable crack growth during fiber-matrix debonding and the sample thickness. The slope of the straight line corresponds to the interfacial fracture toughness

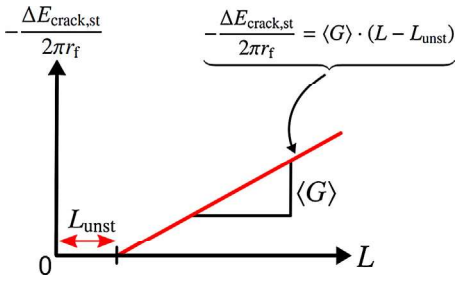

Fig. 7. Schematic illustration: The straight line describes the expected relation between the energy dissipated by stable crack growth during fiber-matrix debonding and the sample thickness L.

$\langle G \rangle$, while the L-axis intercept corresponds to the length of unstable crack propagation L_{unst}. In case only stable crack growth occurs in the debonding process of the fiber, L_{unst} is equal to zero, and the straight line passes through the origin of the diagram.

This expected behavior was examined experimentally by performing single-fiber push-out tests on four samples of the same type (sample PyC-A), which have been thinned to a thickness of 68 μm, 76 μm, 94 μm and 128 μm, respectively (see Table 1). On each sample a minimum of 20 single-fiber push-out tests have been performed. The fiber radii varied from 4.3 to 5.0 μm. The results are shown in Fig. 8.

It can be seen that the data points can be approximated by a linear regression, with an L-axis intercept larger than zero. The error bars represent the standard deviation of the dissipated energy. The error in sample thickness (less than 1 μm) does not appear in the diagram as it is smaller than the size of the data points. The diagram is in total agreement with the expected behavior shown in Fig. 7. The push-out measurements confirm that there is stable and unstable crack propagation involved in the debonding process. The fact that there is a linear relationship between the crack energy and the sample thickness confirms that the length of unstable crack propagation is independent of the

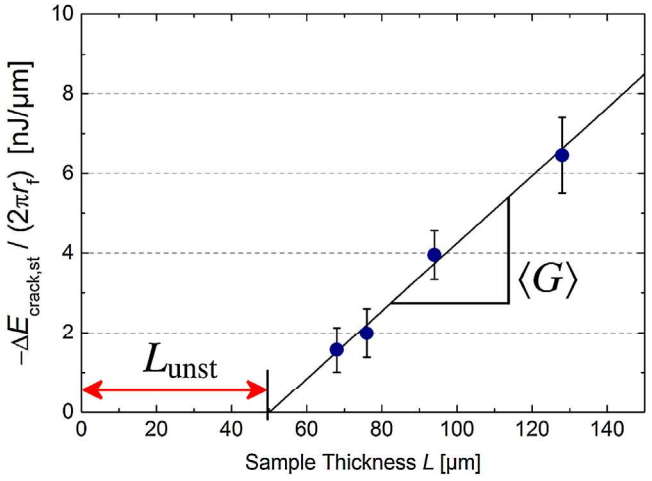

Fig. 8. Diagram of the energy dissipated by stable crack growth (normalized to the individual fiber circumference $2\pi r_f$) during push-out testing as a function of sample thickness L. From the linear regression of the data points, the length of unstable crack growth L_{unst} and the interfacial fracture toughness $\langle G \rangle$ are determined.

sample thickness. With the values determined from experiment, the crack energy is given by

$$-\frac{\Delta E_{crack,st}}{2\pi r_f} = 85\frac{J}{m^2} \cdot (L - 51\,\mu m) \quad (9)$$

By comparing Eq. (9) to Eq. (8), it can be seen that the interfacial fracture toughness $\langle G \rangle$ of the sample PyC-A is equal to $(85 \pm 12)\,J/m^2$ and the length of unstable crack propagation amounts to 51 μm. Hence, the length of unstable crack growth turns out to be in good agreement with the predictions of Kerans and Parthasarathy [3].

In conclusion, the occurrence of stable and unstable crack growth during fiber-matrix debonding in CMC samples has been verified experimentally, and the areas of stable and unstable crack growth have been evaluated.

3.4. Correlation between PyC fiber coating thickness and interfacial fracture toughness

The thickness of the PyC fiber coating is known to influence interfacial properties of SiC/SiC composites, e.g. the interfacial shear strength [8,10]. In the present study, a correlation between the fiber coating thickness and the interfacial fracture toughness is investigated for the first time. To that purpose, the samples PyC-A, PyC-B and PyC-C are investigated by push-out. The composites have been manufactured using the same type of SiC-fiber and similar CVI parameters for the deposition of the PyC coatings and SiC-matrices (see Section 2.1). Apart from the PyC layer thickness, the SEM analysis revealed no differences in microstructure.

Single-fiber push-out tests were performed on two samples of type PyC-B (thickness 60 μm and 85 μm) and on two samples of type PyC-C (thickness 86 μm and 102 μm), in addition to the four samples of PyC-A discussed in Section 3.3. For an overview of the samples investigated, see Table 1.

In Fig. 9, the energy dissipated by stable crack growth (normalized to the individual fiber circumference $2\pi r_f$) is shown as a function of the sample thickness for the sample types PyC-B (red triangles) and PyC-C (green diamonds), together with the samples of type PyC-A (blue dots).

As the intercepts of the linear extrapolations on the L-axis of sample types PyC-B and PyC-C are larger than zero, the diagram confirms that there is stable and unstable crack propagation in these samples, as also observed for sample type PyC-A. The length of unstable crack propagation turns out to be approximately 40 μm for sample PyC-B and 63 μm for sample PyC-C, which again is in agreement with the prediction resulting from stress-based models [3].

The interfacial fracture toughness $\langle G \rangle$ of these samples (corresponding to the slope of the linear extrapolations) amounts to $(208 \pm 53)\,J/m^2$ for PyC-B and $(308 \pm 48)\,J/m^2$ for PyC-C. Macromechanical measurements for comparison could not be performed due to a lack of material to prepare samples of the necessary dimension. However, as end-notched flexure tests on other CVI-SiC/PyC/SiC material published by Choi and Kowalik [25] resulted in a macromechanical fracture toughness in the

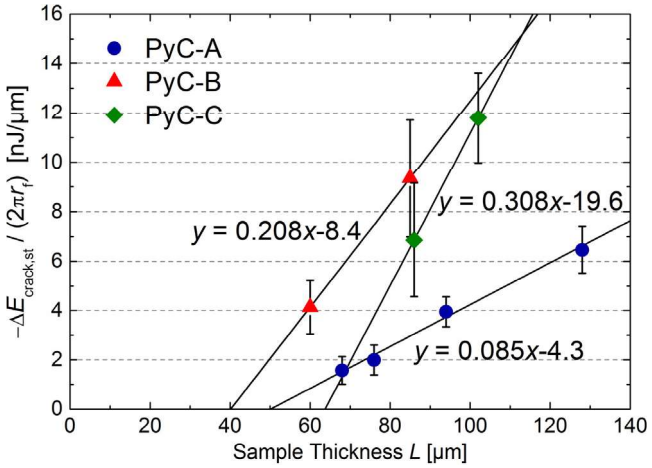

Fig. 9. Diagram of the energy dissipated by stable crack growth (normalized to the individual fiber circumference $2\pi r_f$) during push-out testing as a function of sample thickness L for the samples PyC-A, PyC-B and PyC-C. The interfacial fracture toughness $\langle G \rangle$ and the length of unstable crack growth L_{unst} of each type of sample is given by the slope and the intercept on the L-axis of the linear extrapolations.

range of 200–500 J/m^2, the micromechanical values determined here seem to be of plausible magnitude.

In Fig. 10, the interfacial fracture toughness is plotted versus the PyC coating layer thickness for the three sample types.

An increase of the coating layer thickness by a factor of almost four results in a strong decrease of the interfacial fracture toughness (by almost a factor of four) within the considered range of PyC layer thicknesses. As the data base in the current investigation is limited to three different layer thicknesses, a formal relationship can not be specified. The measured correlation is in good qualitative agreement with the results of Hinoki et al. [8] and Yang et al. [10], which reported a strong decrease in micromechanical interfacial properties with increasing PyC fiber coating thickness. However, in those studies it is the interfacial shear strength which has been evaluated by single-fiber push-out tests.

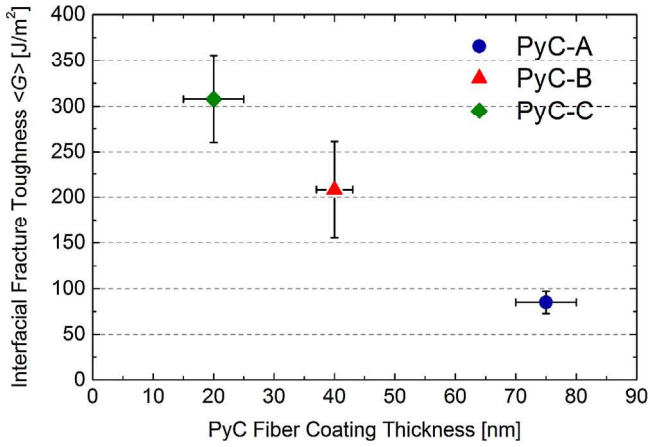

Fig. 10. Effects of the PyC coating layer thickness on the interfacial fracture toughness of SiC/SiC samples.

The decrease of the interfacial fracture toughness with increasing PyC coating thickness may be caused by a higher density of defects in thicker PyC layers as compared to thinner ones. The higher density of defects may lead to a decrease of crack resistance within the PyC layer and thus to a decrease of interfacial fracture toughness. However, the origin of this effect has not been investigated within the current study, and should be analyzed in future works.

4. Conclusions

In the present publication, a new approach to quantify the crack area of stable and unstable crack propagation during single-fiber push-out testing of fiber-reinforced composites is presented. It is applied to SiC-fiber reinforced SiC-matrix composites with PyC fiber coating. By push-out testing of samples with different thicknesses, the occurrence of stable and unstable crack growth during fiber-matrix debonding, which had been predicted, has been verified. The areas of stable and unstable crack growth have been evaluated. The length of unstable crack propagation turned out to be independent of sample thickness.

The more precise quantification of the crack area in single-fiber push-out tests will contribute to a more reliable evaluation of interfacial properties, such as the interfacial fracture toughness.

In the second part of this study, the new approach was applied to investigate a correlation between the PyC fiber coating thickness and the interfacial fracture toughness of SiC/PyC/SiC samples made via CVI technique. It has been found that there is a strong decrease in interfacial fracture toughness with increasing PyC layer thickness within the considered range.

The result underlines that the coating thickness needs to be controlled precisely during manufacturing of the composites and opens up a well-directed and technically easy way to modify the interfacial fracture toughness of SiC/PyC/SiC composites.

Acknowledgements

The authors would like to thank MT Aerospace AG (Dr. K. Handrick) for kindly providing the CMC samples.

References

[1] Naslain R. The design of the fibre-matrix interfacial zone in ceramic matrix composites. Compos Part A 1998;29:1145–55.
[2] Evans A, Zok F. The physics and mechanics of fiber-reinforced brittle-matrix composites. J Mater Sci 1994;29:3857–96.
[3] Kerans R, Parthasarathy T. Theoretical analysis of the fiber pullout and pushout tests. J Am Ceram Soc 1991;74:1585–96.
[4] Marshall D. An indentation method for measuring matrix-fiber frictional stresses in ceramic composites. J Am Ceram Soc 1984;67:C259–60.
[5] Marshall D, Oliver W. Measurement of interfacial mechanical-properties in fiber-reinforced ceramic composites. J Am Ceram Soc 1987;70:542–8.
[6] Lara-Curzio E, Ferber M. Methodology for the determination of the interfacial properties of brittle-matrix composites. J Mater Sci 1994;29:6152–8.
[7] Watanabe K, Kohyama A, Sato S, Serizawa H, Tsunakawa H, Hamada K, et al. Evaluation of interfacial shear strength of C/C composites by means of micro-indentation test. Mater Trans JIM 1996;37:1161–5.

[8] Hinoki T, Zhang W, Kohyama A, Sato S, Noda T. Effect of fiber coating on interfacial shear strength of SiC/SiC by nano-indentation technique. J Nucl Mater 1998;258:1567–71.
[9] Chandra N, Ghonem H. Interfacial mechanics of push-out tests: theory and experiments. Compos Part A 2001;32:575–84.
[10] Yang W, Kohyama A, Noda T, Katoh Y, Hinoki T, Araki H, et al. Interfacial characterization of CVI-SiC/SiC composites. J Nucl Mater 2002;307:1088–92.
[11] Rebillat F, Lamon J, Naslain R, Lara-Curzio E, Ferber M, Theodore M. Properties of multilayered interphases in SiC/SiC chemical-vapor-infiltrated composites with “weak” and “strong” interfaces. J Am Ceram Soc 1998;81:2315–26.
[12] Rebillat F, Lamon J, Naslain R, Lara-Curzio E, Ferber M, Besmann T. Interfacial bond strength in SiC/C/SiC composite materials, as studied by single-fiber push-out tests. J Am Ceram Soc 1998;81:965–78.
[13] Rebillat F, Lamon J, Naslain R. Multilayered interphases in SiC/SiC Composites: influences of the interfacial bond strength on the interfacial characteristics. Key Eng Mater 1999;164–165:361–4.
[14] Rebillat F, Lamon J, Guette A. The concept of a strong interface applied to SiC/SiC composites with a BN interphase. Acta Mater 2000;48:4609–18.
[15] Mueller WM, Moosburger-Will J, Sause MGR, Horn S. Microscopic analysis of single-fiber push-out tests on ceramic matrix composites performed with berkovich and flat-end indenter and evaluation of interfacial fracture toughness. J Eur Ceram Soc 2013;33:441–51.
[16] Mueller WM. Faser-Matrix-Anbindung in keramischen Faserverbundwerkstoffen: Einzelfaser-Push-out Untersuchungen und Entwicklung einer Siliziumoxycarbid-Faserbeschichtung. University of Augsburg; 2014. Ph.D. thesis.
[17] Greisel M, Jaeger J, Moosburger-Will J, Sause MGR, Mueller WM, Horn S. Influence of residual thermal stress in carbon fiber-reinforced thermoplastic composites on interfacial fracture toughness evaluated by cyclic single-fiber push-out tests. Compos Part A: Appl Sci Manuf 2014;66:117–27.
[18] Battisti A, de los Ojos DE, Ghisleni R, Brunner AJ. Single fiber push-out characterization of interfacial properties of hierarchical cnt-carbon fiber composites prepared by electrophoretic deposition. Compos Sci Technol 2014;95:121–7.
[19] Jaeger J, Sause MGR, Burkert F, Moosburger-Will J, Greisel M, Horn S. Influence of plastic deformation on single-fiber push-out tests of carbon fiber reinforced epoxy resin. Compos Part A: Appl Sci Manuf 2015;71:157–67.
[20] Suresh S. Fatigue of materials, vol. 8 of cambridge solid state science series. Cambridge University Press; 1994.
[21] Gross D, Seelig T. Bruchmechanik. 5th ed. Springer London, Limited; 2011.
[22] Griffith AA. The phenomena of rupture and flow in solids. Philos Trans R Soc Lond 1921;221:163–98.
[23] Jero P, Kerans R, Parthasarathy T. Effect of interfacial roughness on the frictional stress measured using pushout tests. J Am Ceram Soc 1991;74:2793–801.
[24] Kerans R, Parthasarathy T, Rebillat F, Lamon J. Interface properties in high-strength Nicalon/C/SiC composites, as determined by rough surface analysis of fiber push-out tests. J Am Ceram Soc 1998;81:1881–7.
[25] Choi S, Kowalik R. Interlaminar crack growth resistances of various ceramic matrix composites in mode I and mode II loading. J Eng Gas Turbines Power 2008;130, 031301-1–031301-8.